amount of decrease was observed only when the cutoff length was changed from 7.8 Å to 6.6 Å. Corresponding to the larger change in cutoff length to achieve the same amount of decrease of the coefficient, the number of the springs eliminated by the change in cutoff length was larger (1495 vs. 231). This result further supports the idea that there were more springs in the conventional elastic network model than in our model that did not critically influence the molecular motions.

The results presented here suggest that the short-distance interactions between two residues in our elastic network model have a potentially greater influence on the molecular motions than those in the conventional elastic network model, and thus that our definition of the distance between two residues is more effective than that in the conventional elastic network model in extracting or sorting such influential interactions, which is the major aim of this study.

Identifying key interactions for conformational change by NMA

Tama et al. (59) performed NMAs of the (conventional) elastic network models of proteins whose open and closed forms were solved by x-ray crystallography. They compared the atomic displacements in the conformational change from open to closed and closed to open forms with those in the normal modes. They found that the elastic network model for the open form generally had a normal mode in which the atomic displacements were close to those in the conformational change, whereas that for the closed form did not. In the case of integrin, there are two forms, that is, the bent form and the extended form. The former corresponds to the closed form, and the latter to the open form. The x-ray crystal structure was solved only for the bent form. Thus, if we consider the study by Tama et al. (59), what we did corresponds to the study to find the normal modes of the closed form of a protein that directed the molecule toward the open form. We found that the normal modes involved in the conformational change were newly generated by reducing the cutoff length until the correlation coefficients dropped drastically. Thus, our approach may be regarded as a possible solution for finding the normal modes of the closed form of a protein that direct the molecular structure toward the open form.

Instead of reducing the cutoff length, we can "manually" eliminate the interactions between domains of the elastic network model so that the extension of the molecule becomes easier. Assuming the cutoff length $r_c = 5$ Å, we performed NMA of the elastic network model. When all springs between the hybrid domain and the EGF/βTD domains were eliminated from this model, the correlation coefficient dropped from 0.54 (Fig. 2, *open circles*) to 0.34, and the lowest-frequency normal mode was similar to that shown in Fig. 3 *a* (with similarity of 0.75). This suggests that the "manual" elimination of interactions has an effect similar to the reduction of the cutoff length. However, without prior knowledge, it is difficult to decide which interactions should be eliminated.

Mutation experiments

Our calculations suggested that the interactions between Arg^{633} and the nonbonded nearby residues had to be eliminated for the structural rearrangement of integrin from the bent to the extended form to occur. Our calculations also suggested that the extension of integrin would be enhanced once the interactions were eliminated. To examine our predictions, specific interactions involving Arg^{633} were disrupted by mutating amino acid residues involved in the interactions.

Mutant $\alpha_{IIb}\beta_3$ was transiently expressed on the mammalian CHO cell surface and FITC-labeled fibrinogen-binding to these cells was examined. As shown in Fig. 7 *a*, wild-type $\alpha_{IIb}\beta_3$ expressed on the CHO cell surface was in a low-af-

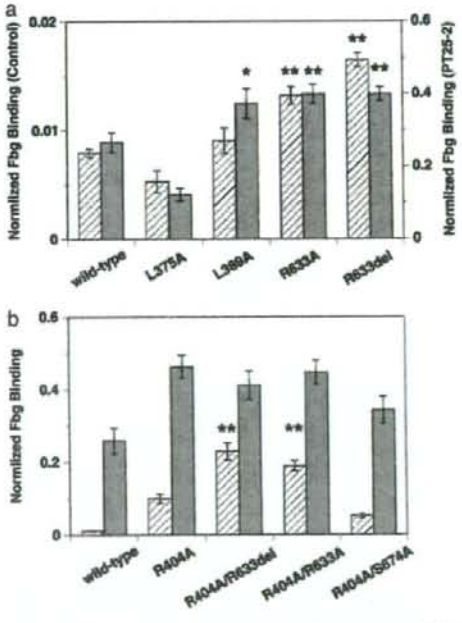

FIGURE 7 Average amount of FITC-labeled Fbg bound to CHO cells expressing wild-type or mutated $\alpha_{IIb}\beta_3$ obtained from six separate experiments. The amount of Fbg in the presence of control antibody (*hatched bars*) and PT25-2 (*shaded bars*) is shown separately in arbitrary units with error bars. (*a*) Results for mutations at the residues involved in the Arg^{633}-mediated interactions are compared with those for the wild-type. Amino acid residues Leu^{375}, Leu^{389}, and Arg^{633} in the β_3-chain were either mutated to Ala (*L375A*, *L389A*, and *R633A*) or deleted (*R633del*). The amount of Fbg in the presence of the control antibody and PT25-2 is shown in the left and right axes, respectively. Mutants that showed a statistically significant increase in binding from the wild-type are indicated by asterisks: $*p < 0.05$; $**p < 0.01$. (*b*) Results for single mutation of Arg^{404} in the β_3-chain (*R404A*) and double mutations of Arg^{404} in combination with either Arg^{633} (*R404A/R633A*, *R404A/R633del*) or Ser^{674} (*R404A/S674A*) are shown and compared with those for the wild-type. Mutants that showed significant increase in binding from the wild-type are indicated by asterisks: $**p < 0.01$.

finity state and did not bind to fibrinogen significantly unless activated by mAb PT25-2, which brought up the binding by ~33-fold. It has previously been shown that the mAb PT25-2 binds to the β-propeller domain of α_{IIb}-chain of integrin in platelets and induces the binding of integrin to fibrinogen (43,60). In contrast to the independent mutation of Leu^{375} or Leu^{389} to Ala, where the binding to fibrinogen was not affected so much, mutation of Arg^{633} to Ala, or its complete deletion, significantly increased the binding ($p < 0.01$). Activation with PT25-2 gave similar results, except that the L389A mutation showed a significant increase in binding ($p < 0.05$). These results indicate that the interactions involving the side chain of Arg^{633} are indeed important for constraining $\alpha_{IIb}\beta_3$ in a low-affinity state, as we predicted.

The mutations L375A and L389A did not activate $\alpha_{IIb}\beta_3$ (actually L375A with PT25-2 deactivated it, with $p < 0.01$). Because the degree of expression of integrin on the cell surface was not affected by these mutations, it is not probable that the mutations caused global conformational change. To find the reason for the low activation, we checked the thermal fluctuations of side-chain atoms in the arginine residues derived from the B-factor of the x-ray crystal structure. There are 62 arginines in the x-ray crystal structure. In most of the residues, the thermal fluctuations of the side-chain atoms farther away from the C_α atom are larger ($C_\beta < C_\gamma < C_\delta < \ldots$), suggesting the inherent flexibility of the side chain. Due to this flexibility, the side-chain atoms of Arg^{633} might be able to find new interaction sites in the mutated residue or in the nearby residues when Leu^{375} or Leu^{389} were mutated. In the case of L375A, the newly generated interactions might turn out to be stronger than the original and, as a result, $\alpha_{IIb}\beta_3$ might be further deactivated.

Our experimental results showed that complete elimination of the interactions involving Arg^{633} by deletion was not sufficient to fully activate $\alpha_{IIb}\beta_3$. According to our calculation, the elimination of Arg^{633}-mediated interactions alone would allow only halfway extension of integrin (Fig. 5 *b*); in other words, Arg^{633} is the key residue to initiate the extension, but not the key residue to complete the extension. Thus, the results from the mutational studies are consistent with our calculations. The calculation further showed that complete extension would be achieved if the interactions between the hybrid domain and EGF domains involving Arg^{404} were also eliminated (Fig. 5 *a*). To verify this calculation result, we introduced mutations on both Arg^{404} and Arg^{633} at the same time. Arg^{404} was mutated to Ala and Arg^{633} was either mutated to Ala or deleted. As a reference, we performed a double mutation on Arg^{404} and Ser^{674}, both of which were mutated to Ala, as well as a single mutation of Arg^{404} to Ala. The mutation of Ser^{674} is already known to have little effect on the activation, as discussed above. The results of the double mutations are almost exactly as we expected based on our calculations, as shown in Fig. 7 *b*. Compared to the single mutation R404A, the double mutations R404A/R633X (where X is A or del) clearly had larger effects ($p < 0.01$), which is in contrast to the effect of R404A/S674A, where the activity of integrin was not significantly different from the single mutations. The comparison between R404A/R633X and R404A/S674A demonstrates the importance of Arg^{633} again. These experimental and computational results suggest that the interactions at multiple interfaces have to be disrupted to achieve full activation as well as full extension.

It was demonstrated that $\alpha_V\beta_3$ and $\alpha_{IIb}\beta_3$ integrins are different in their signaling mechanisms (40). This difference may be partially explained by the different interactions between the cytoplasmic α and β tails, in addition to the difference between the molecules that may associate with the specific α cytoplasmic tails. Another report showed that extracellular calf-2/(EGF-4 and βTD) interface interactions affect manganese-induced activation differently in two β_3 integrins (61). These reports suggest that the α/β interface interactions have a significant impact on integrin activation and are responsible for the differential regulation in two β_3 integrins. Thus, the Arg^{633} mutations may not necessarily have the same effect on the $\alpha_V\beta_3$-ligand interaction as on the

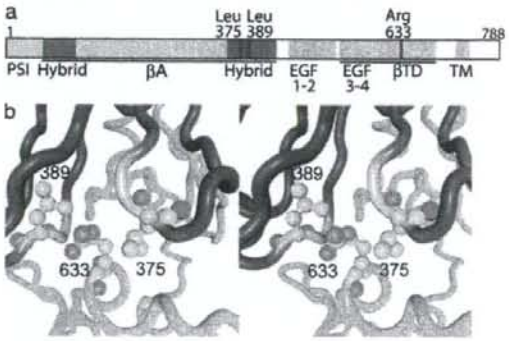

c

	375	389	633
β1	K	I	Q/E
β2	x	V	x
β3	L/Q	L	R/H/Q
β4	x	E/Q	E/D
β5	Q	L	x
β6	N/S	M	D
β7	x	V	x
β8	P	V	S/T

x : more than two types of aa
- : gap in the alignment

FIGURE 8 Conservation patterns of amino acid residues among different integrin β-chains at positions corresponding to positions 375, 389, and 633 of *H. sapiens* integrin β-chain. (*a*) A diagram of integrin β-chain to show domain organization and the location of residues 375, 389, and 633. Black bars below the diagram indicate regions observed with x-ray crystal structure. (*b*) Stereo figure of local structure around the three residues, showing that Arg^{633} is sandwiched by Leu^{375} and Leu^{389}. (*c*) Conservation pattern of residues in the three positions of mammalian integrin β-chain extracted from the multiple sequence alignment in Fig. 9. A slash in the column indicates that the position is occupied by one of the two or three amino acid residues, and x indicates that the position is not conserved in the group.

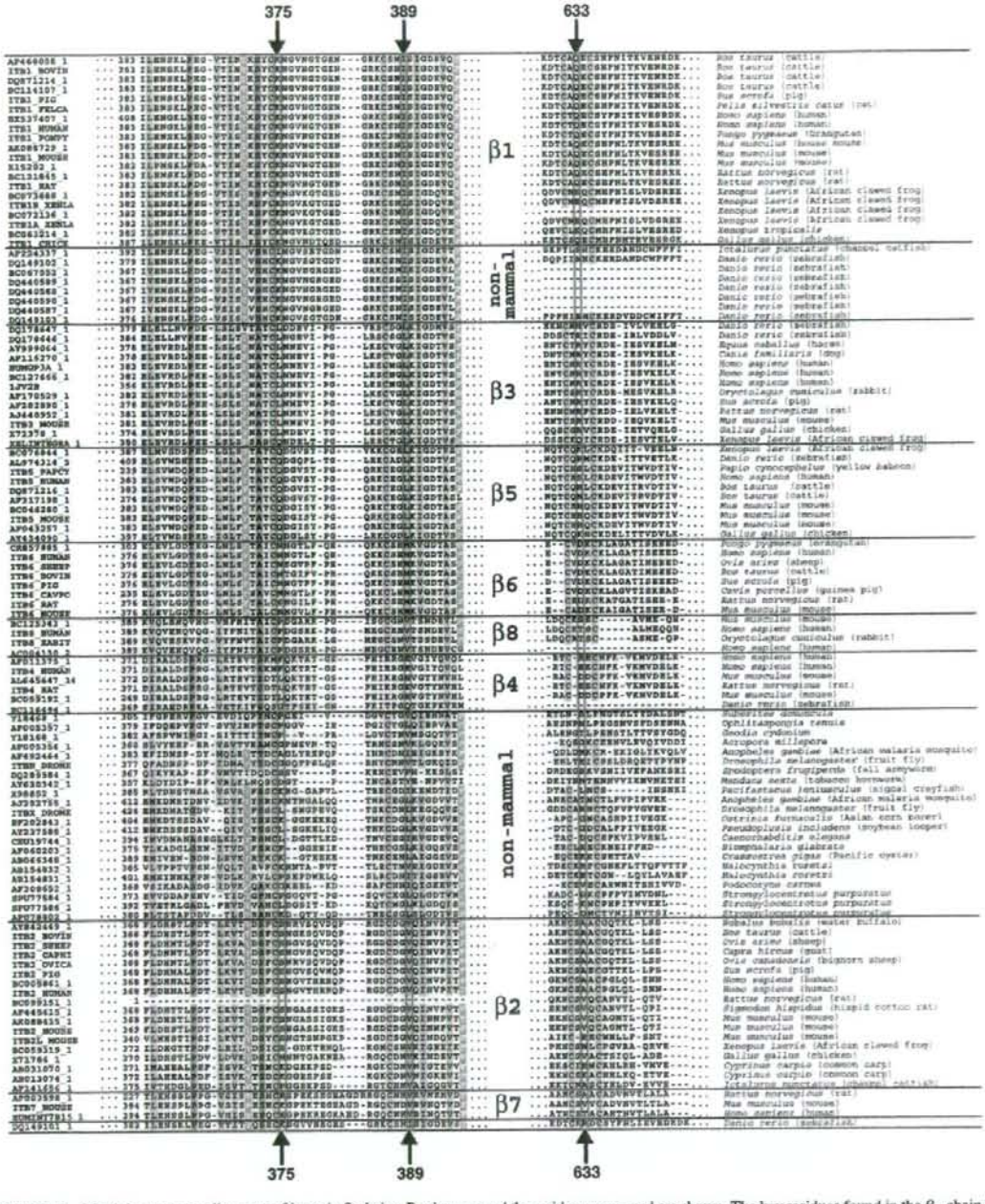

FIGURE 9 Multiple-sequence alignment of integrin β-chains. Regions around the residues concerned are shown. The key residues found in the β_3-chain by NMA on *H. sapiens* integrin $\alpha_V\beta_3$ and residues at homologous sites are boxed in red. Well conserved residues and cysteine residues in all the chains are highlighted. Identifications of each sequence in Genbank/UniProt/PDB are described on the left and the name of the species that the sequence is derived from is described on the right. The order of amino acid sequences is based on the sequence identity, and a horizontal bar separates groups in β-chains. The alignment around position 633 of β_4- and nonmammal chains was manually adjusted after automatic multiple-sequence alignment.

$\alpha_{IIb}\beta_3$-fibrinogen interaction observed in this study. However, the primary interdomain interactions that directly constrain $\alpha_V\beta_3$ integrin to the bent form in the crystal structure will be those of the hybrid domain with EGF and βTD domains, in which the interactions of Arg^{633} are included, and not those at the α/β interface. Thus, it is reasonable to assume that disrupting the Arg^{633}-mediated interactions has similar effects on the activation of $\alpha_V\beta_3$ as well.

Conservation patterns of residues in key interactions in the integrin β-chain

NMAs and mutation experiments on integrin suggested that the interactions of Arg^{633} in the β_3-chain with nearby nonbonded residues work as a snap to keep integrin in the bent form. Among the nearby residues, two leucine residues interact with Arg^{633} in an interesting manner, that is, they sandwich the side chain of Arg^{633} (Fig. 8 *b*). We checked the conservation pattern of these residues in homologous integrin β-chain sequences.

From the amino acid sequence databases, 113 sequences homologous to the *H. sapiens* integrin β_3-chain were retrieved and were clustered into 10 groups by a phylogenetic tree built on a multiple-sequence alignment (Fig. 9). Mammalian integrin β-chains are known to be classified into eight groups based on sequence similarity, ligand specificity, and expressed cells (1). Our results included two clusters of nonmammalian integrin β-chains, and eight other groups were consistent with the previous study. The set of key residues was conserved as Leu/Leu/Arg only in the integrin β_3-chain, and in other β-chains, the evolutionarily corresponding positions were either conserved with different amino acid residues or not conserved (Fig. 8 *c*).

Arginine has one of the longest aliphatic side chains in 20 amino acids, and hence, possible interactions between Leu and Arg are hydrophobic ones using aliphatic side chains (Fig. 8 *b*). The conservation patterns of other β-chains are dissimilar to those of the β_3-chain, which suggests that other β-chains may have different molecular mechanisms for the conformational transition or do not undergo a conformational change at all. β_1- and β_2-chains are known to undergo a similar type of bent-to-extended conformational transition, and we surmise that the molecular detail of the mechanism is different from that in β_3-chain.

CONCLUSION

The conformational change of integrin from the bent to the extended forms was studied by NMA of the elastic network model. The calculations revealed the key residues for the conformational change, and their importance was confirmed by the experiment. Multiple sequence alignment showed that the characteristic pattern of residues (Leu/Leu/Arg) was conserved only in the integrin β_3-chain, suggesting that the mechanism of the conformational change from the bent to the extended forms studied here is unique to the chain.

A pathway for the conformational change was speculated from the calculations, which is summarized as follows. The first step is the motion of the βTD as a whole (shown in Fig. 3 *b*), which is perhaps brought up by a signal from inside the cell (inside-out signaling). This motion involves the displacement of Arg^{633} in the β_3-chain, whose side chain is sandwiched by two leucine residues in the x-ray crystal structure. By this motion, the interactions of Arg^{633} with nearby nonbonded residues will be eliminated. Once the interactions of Arg^{633} are eliminated, the molecular motions change quite drastically. Specifically, the motions of the hybrid domain in the β_3-chain become dominant (Fig. 3 *a*). The motions will enhance the separation of the hybrid domain from the EGF domains and will contribute to the elimination of the interactions between these domains. If the interactions are eliminated, further drastic conformational change becomes easier, and the molecule will extend (Fig. 5 *a*).

We thank Ms. Sonomi Ito for her excellent technical assistance.

A.M., K.I., and K.Y. were supported by CREST, Japan Science and Technology Agency. T.K. was supported by a Health and Labor Science Research Grant for Research on Regulatory Science of Pharmaceuticals and Medical Devices from the Ministry of Health, Labor and Welfare, and by a Grant for Leading Project for Biosimulation from the Ministry of Education, Culture, Sports, Science and Technology of Japan.

REFERENCES

1. Hynes, R. O. 2002. Integrins: bidirectional, allosteric signaling machines. *Cell.* 110:673–687.
2. Ginsberg, M. H., D. Xiaoping, T. E. O'Toole, J. C. Loftus, and E. F. Plow. 1993. Platelet integrins. *Thromb. Haemost.* 70:87–93.
3. Xiong, J.-P., T. Stehle, B. Diefenbach, R. Zhang, R. Dunker, D. L. Scott, A. Joachimiak, S. L. Goodman, and M. A. Arnaout. 2001. Crystal structure of the extracellular segment of integrin $\alpha_V\beta_3$. *Science.* 294: 339–345.
4. Nermut, M. V., N. M. Green, P. Eason, S. S. Yamada, and K. M. Yamada. 1988. Electron microscopy and structural model of human fibronectin receptor. *EMBO J.* 7:4093–4099.
5. Du, X., M. Gu, J. W. Weisel, C. Nagaswami, J. S. Bennett, R. Bowditch, and M. H. Ginsberg. 1993. Long range propagation of conformational changes in integrin $\alpha_{IIb}\beta_3$. *J. Biol. Chem.* 268:23087–23092.
6. Takagi, J., H. P. Erickson, and T. A. Springer. 2001. C-terminal opening mimics "inside-out" activation of integrin $\alpha_5\beta_1$. *Nat. Struct. Biol.* 8: 412–416.
7. Takagi, J., B. M. Petre, T. Walz, and T. A. Springer. 2002. Global conformational rearrangements in integrin extracellular domains in outside-in and inside-out signaling. *Cell.* 110:599–611.
8. Brooks, B., and M. Karplus. 1983. Harmonic dynamics of proteins: normal modes and fluctuations in bovine pancreatic trypsin inhibitor. *Proc. Natl. Acad. Sci. USA.* 80:6571–6575.
9. Go, N., T. Noguti, and T. Nishikawa. 1983. Dynamics of a small globular protein in terms of low-frequency vibrational modes. *Proc. Natl. Acad. Sci. USA.* 80:3696–3700.
10. Levitt, M., C. Sander, and P. S. Stern. 1985. Protein normal-mode dynamics: trypsin inhibitor, crambin, ribonuclease and lysozyme. *J. Mol. Biol.* 181:423–447.

11. Tirion, M. M. 1996. Large amplitude elastic motions in proteins from a single-parameter, atomic analysis. *Phys. Rev. Lett.* 77:1905–1908.
12. Bahar, I., A. R. Atilgan, and B. Erman. 1997. Direct evaluation of thermal fluctuations in proteins using a single-parameter harmonic potential. *Fold. Des.* 2:173–181.
13. Tama, F., and C. L. Brooks III. 2002. The mechanism and pathway of pH induced swelling in cowpea chlorotic mottle virus. *J. Mol. Biol.* 318:733–747.
14. Tama, F., M. Valle, J. Frank, and C. L. Brooks III. 2003. Dynamic reorganization of the functionally active ribosome explored by normal mode analysis and cryo-electron microscopy. *Proc. Natl. Acad. Sci. USA.* 100:9319–9323.
15. Tama, F., and C. L. Brooks III. 2005. Diversity and identity of mechanical properties of icosahedral viral capsids studied with elastic network normal mode analysis. *J. Mol. Biol.* 345:299–314.
16. Wang, Y., A. J. Rader, I. Bahar, and R. L. Jernigan. 2004. Global ribosome motions revealed with elastic network model. *J. Struct. Biol.* 147:302–314.
17. Kim, M. K., R. L. Jernigan, and G. S. Chirikjian. 2003. An elastic network model of HK97 capsid maturation. *J. Struct. Biol.* 143:107–117.
18. Hinsen, K. 1998. Analysis of domain motions by approximate normal mode calculations. *Proteins.* 33:417–429.
19. Nishikawa, T., and N. Go. 1987. Normal mode of vibration in bovine pancreatic trypsin inhibitor and its mechanical property. *Proteins.* 2:308–329.
20. Durand, P., G. Trinquier, and Y.-H. Sanejouand. 1994. A new approach for determining low-frequency normal modes in macromolecules. *Biopolymers.* 34:759–771.
21. Lin, D., A. Matsumoto, and N. Go. 1997. Normal mode analysis of a double-stranded DNA dodecamer d(CGCGAATTCGCG). *J. Chem. Phys.* 107:3684–3690.
22. Matsumoto, A., M. Tomimoto, and N. Go. 1999. Dynamical structure of transfer RNA by normal mode analysis. *Eur. Biophys. J.* 28:369–379.
23. Matsumoto, A., and N. Go. 1999. Dynamic properties of double-stranded DNA by normal mode analysis. *J. Chem. Phys.* 110:11070–11075.
24. Matsumoto, A., and W. K. Olson. 2002. Sequence-dependent motions of DNA: a normal mode analysis at the base-pair level. *Biophys. J.* 83:22–41.
25. Matsumoto, A., I. Tobias, and W. Olson. 2005. Normal-mode analysis of circular DNA at the base-pair level. 1. Comparison of computed motions with the predicted behavior of an ideal elastic rod. *J. Chem. Theory Comput.* 1:117–129.
26. Matsumoto, A., I. Tobias, and W. Olson. 2005. Normal-mode analysis of circular DNA at the base-pair level. 2. Large-scale configurational transformation of a naturally curved molecule. *J. Chem. Theory Comput.* 1:130–142.
27. Matsumoto, A., and W. K. Olson. 2006. Predicted effects of local conformational coupling and external restraints on the torsional properties of single DNA molecules. *Multiscale Model. Simul.* 5:1227–1247.
28. Miyashita, O., J. N. Onuchic, and P. G. Wolynes. 2003. Nonlinear elasticity, proteinquakes, and the energy landscapes of functional transitions in proteins. *Proc. Natl. Acad. Sci. USA.* 100:12570–12575.
29. Tama, F., W. Wriggers, and C. L. Brooks III. 2002. Exploring global distortions of biological macromolecules and assemblies from low-resolution structural information and elastic network theory. *J. Mol. Biol.* 321:297–305.
30. Tama, F., O. Miyashita, and C. L. Brooks III. 2004. Flexible multi-scale fitting of atomic structures into low-resolution electron density maps with elastic network normal mode analysis. *J. Mol. Biol.* 337:985–999.
31. Hinsen, K., N. Reuter, J. Navaza, D. L. Stokes, and J. J. Lacapere. 2005. Normal mode-based fitting of atomic structure into electron density maps: application to sarcoplasmic reticulum Ca-ATPase. *Biophys. J.* 88:818–827.
32. McLachlan, A. D. 1979. Gene duplications in the structural evolution of chymotrypsin. *J. Mol. Biol.* 128:49–79.
33. The UniProt Consortium. 2007. The Universal Protein Resource (UniProt). *Nucleic Acids Res.* 35:D193–D197.
34. Sugawara, H., T. Abe, T. Gojobori, and Y. Tateno. 2007. DDBJ working on evaluation and classification of bacterial genes in INSDC. *Nucleic Acids Res.* 35:D13–D15.
35. Altschul, S. F., T. L. Madden, A. A. Schaffer, J. Zhang, Z. Zhang, W. Miller, and D. J. Lipman. 1997. Gapped BLAST and PSI-BLAST: a new generation of protein database search programs. *Nucleic Acids Res.* 25:3389–3402.
36. Barton, G. J., and M. J. Sternberg. 1987. A strategy for the rapid multiple alignment of protein sequences. Confidence levels from tertiary structure comparisons. *J. Mol. Biol.* 198:327–337.
37. Henikoff, S., and J. G. Henikoff. 1992. Amino acid substitution matrices from protein blocks. *Proc. Natl. Acad. Sci. USA.* 89:10915–10919.
38. Saitou, N., and M. Nei. 1987. The neighbor-joining method: a new method for reconstructing phylogenetic trees. *Mol. Biol. Evol.* 4:406–425.
39. Kimura, M. 1983. The Neutral Theory of Molecular Evolution. Cambridge University Press, London.
40. Ahrens, I. G., N. Moran, K. Aylward, G. Meade, M. Moser, D. Assefa, D. J. Fitzgerald, C. Bode, and K. Peter. 2006. Evidence for a differential functional regulation of the two β_3-integrins $\alpha_V\beta_3$ and $\alpha_{IIb}\beta_3$. *Exp. Cell Res.* 312:925–937.
41. Calvete, J. J. 2004. Structures of integrin domains and concerted conformational changes in the bidirectional signaling mechanism of $\alpha_{IIb}\beta_3$. *Exp. Biol. Med. (Maywood).* 229:732–744.
42. Ylanne, J., M. Hormia, M. Jarvinen, T. Vartio, and I. Virtanen. 1988. Platelet glycoprotein IIb/IIIa complex in cultured cells. Localization in focal adhesion sites in spreading HEL cells. *Blood.* 72:1478–1486.
43. Tokuhira, M., M. Handa, T. Kamata, A. Oda, M. Katayama, Y. Tomiyama, M. Murata, Y. Kawai, K. Watanabe, and Y. Ikeda. 1996. A novel regulatory epitope defined by a murine monoclonal antibody to the platelet GPIIb-IIIa complex ($\alpha_{IIb}\beta_3$ integrin). *Thromb. Haemost.* 76:1038–1046.
44. Kamata, T., A. Irie, M. Tokuhira, and Y. Takada. 1996. Critical residues of integrin αIIb subunit for binding of $\alpha_{IIb}\beta_3$ (glycoprotein IIb-IIIa) to fibrinogen and ligand-mimetic antibodies (PAC-1, OP-G2, and LJ-CP3). *J. Biol. Chem.* 271:18610–18615.
45. Crowe, D. T., H. Chiu, S. Fong, and I. L. Weissman. 1994. Regulation of the avidity of integrin $\alpha_4\beta_7$ by the β_7 cytoplasmic domain. *J. Biol. Chem.* 269:14411–14418.
46. Hughes, P. E., T. E. O'Toole, J. Ylanne, S. J. Shattil, and M. H. Ginsberg. 1995. The conserved membrane-proximal region of an integrin cytoplasmic domain specifies ligand binding affinity. *J. Biol. Chem.* 270:12411–12417.
47. Hughes, P. E., F. Diaz-Gonzalez, L. Leong, C. Wu, J. A. McDonald, S. J. Shattil, and M. H. Ginsberg. 1996. Breaking the integrin hinge. *J. Biol. Chem.* 271:6571–6574.
48. Kim, M., C. V. Carman, and T. A. Springer. 2003. Bidirectional transmembrane signaling by cytoplasmic domain separation in integrins. *Science.* 301:1720–1725.
49. Lu, C. F., and T. A. Springer. 1997. The α subunit cytoplasmic domain regulates the assembly and adhesiveness of integrin lymphocyte function-associated antigen-1. *J. Immunol.* 159:268–278.
50. Lu, C., J. Takagi, and T. A. Springer. 2001. Association of the membrane proximal regions of the α and β subunit cytoplasmic domains constrains an integrin in the inactive state. *J. Biol. Chem.* 276:14642–14648.
51. O'Toole, T. E., D. Mandelman, J. Forsyth, S. J. Shattil, E. F. Plow, and M. H. Ginsberg. 1991. Modulation of the affinity of integrin $\alpha_{IIb}\beta_3$ (GPIIb-IIIa) by the cytoplasmic domain of α_{IIb}. *Science.* 254:845–847.

52. O'Toole, T. E., Y. Katagiri, R. J. Faull, K. Peter, R. Tamura, V. Quaranta, J. C. Loftus, S. J. Shattil, and M. H. Ginsberg. 1994. Integrin cytoplasmic domains mediate inside-out signal transduction. *J. Cell Biol.* 124:1047–1059.

53. Ylanne, J., Y. Chen, T. E. O'Toole, J. C. Loftus, Y. Takada, and M. H. Ginsberg. 1993. Distinct functions of integrin α and β subunit cytoplasmic domains in cell spreading and formation of focal adhesions. *J. Cell Biol.* 122:223–233.

54. Xiong, Y.-M., J. Chen, and L. Zhang. 2003. Modulation of CD11b/CD18 adhesive activity by its extracellular, membrane-proximal regions. *J. Immunol.* 171:1042–1050.

55. Calderwood, D. A., R. Zent, R. Grant, D. J. G. Rees, R. O. Hynes, and M. H. Ginsberg. 1999. The talin head domain binds to integrin β subunit cytoplasmic tails and regulates integrin activation. *J. Biol. Chem.* 274:28071–28074.

56. Calderwood, D. A., B. Yan, J. M. de Pereda, B. G. Alvarez, Y. Fujioka, R. C. Liddington, and M. H. Ginsberg. 2002. The phosphotyrosine binding-like domain of talin activates integrins. *J. Biol. Chem.* 277: 21749–21758.

57. Vinogradova, O., A. Velyvis, A. Velyviene, B. Hu, T. A. Haas, E. F. Plow, and J. Qin. 2002. A structural mechanism of integrin $\alpha_{IIb}\beta_3$ "inside-out" activation as regulated by its cytoplasmic face. *Cell.* 110: 587–597.

58. Kamata, T., K. K. Tieu, A. Irie, T. A. Springer, and Y. Takada. 2001. Amino acid residues in the α_{IIb} subunit that are critical for ligand binding to integrin $\alpha_{IIb}\beta_3$ are clustered in the β-propeller model. *J. Biol. Chem.* 276:44275–44283.

59. Tama, F., and Y.-H. Sanejouand. 2001. Conformational change of proteins arising from normal mode calculations. *Protein Eng.* 14:1–6.

60. Puzon-McLaughlin, W., T. Kamata, and Y. Takada. 2000. Multiple discontinuous ligand-mimetic antibody binding sites define a ligand binding pocket in integrin $\alpha_{IIb}\beta_3$. *J. Biol. Chem.* 275:7795–7802.

61. Kamata, T., M. Handa, Y. Sato, Y. Ikeda, and S. Aiso. 2005. Membrane-proximal α/β stalk interactions differentially regulate integrin activation. *J. Biol. Chem.* 280:24775–24783.

62. Humphrey, W., A. Dalke, and K. Schulten. 1996. VMD: visual molecular dynamics. *J. Mol. Graph.* 14:33–38.

血栓止血誌 19(6) : 774–778, 2008

◆特集：血小板を作ろう　総説◆

血小板代替物

半田　誠[*1]，岡村陽介[*2]，武岡真司[*2]，
池田康夫[*3]

半田　誠

1976年3月　慶應義塾大学医学部卒業
1980年7月　慶應義塾大学助手（血液内科学）
1991年4月　慶應義塾大学専任講師
（輸血センター室長）
2000年4月　慶應義塾大学助教授
（輸血センター室長）
2007年4月　慶應義塾大学准教授
（輸血・細胞療法部長）

Platelet substitutes

Makoto HANDA[*1], Yosuke OKAMURA[*2], Shinji TAKEOKA[*2], Yasuo IKEDA[*3]

Key words: Platelet substitute, Platelet transfusion, Fibrinogen-coated albumin particles, H12-coated liposomes, ADP encapsulation

はじめに

血小板は一次血栓形成を通じて生体の止血機構の中心をなし，その量的・質的異常により惹起される出血の予防や治療に対し唯一信頼できる手段は血小板輸血である．高度な医療に必須な血小板の必要量は将来も減少することはなく，一方，人口減と高齢化に伴う献血者数の低下などでその供給量の減少が予想されること，そして，短い期限（4日）で厳密な保存条件が要求されることから災害時等への緊急対応が極めて困難であること，などから液状の血小板濃厚液に代わる安定的な製造物（血小板代替物，platelet substitutes）の開発が行われてきた．

血小板代替物の種類（図1）

広義の血小板代替物は，血小板そのものを加工した血小板由来産物と，血小板以外の構成成分から成り立った人工産物に大別され，後者がいわゆる狭義の血小板代替物（人工血小板：artificial platelets）である[1]．前者の開発の歴史は古く，米国において軍事目的のための国防費による研究が実に50年代から始まった．その結果，固定血小板や凍結乾燥血小板，あるいは凍結乾燥した血小板膜断片（infusible platelet membrane : IPM）などが開発され，IPMは初期臨床研究（フェーズI/II）に供された．一方，後者は生体適合性のある担体（赤血球，アルブミン微粒子，リン脂質小胞体：リポソームなど）を用い，その表面に血小板受容体やリガンドを結合させたもので，90年代初めにフィブリノゲンやその合成ペプチド（RGD）をコートした赤血球（Thromboerythrocyte）が先駆けとなり，いくつかの微粒子が開発され，フィブリノゲンを表面固定したアルブミン微粒子（Synthocyte™

[*1]慶應義塾大学輸血・細胞療法部〔〒160-8582 新宿区信濃町35〕
Department of Transfusion Medicine & Cell Therapy, School of Medicine, Keio University
〔35 Shinanomachi, Shinjuku, Tokyo 160-8582, Japan〕
Tel: 03-3353-1211 (ext. 62123)　Fax: 03-3353-9706　e-mail: mhanda@sc.itc.keio.ac.jp
[*2]早稲田大学理工学術院
Department of Life Science and Medical Bioscience, Graduate School of Advanced Science and Engineering, Waseda University
[*3]慶應義塾大学内科
Department of Internal Medicine, School of Medicine, Keio University

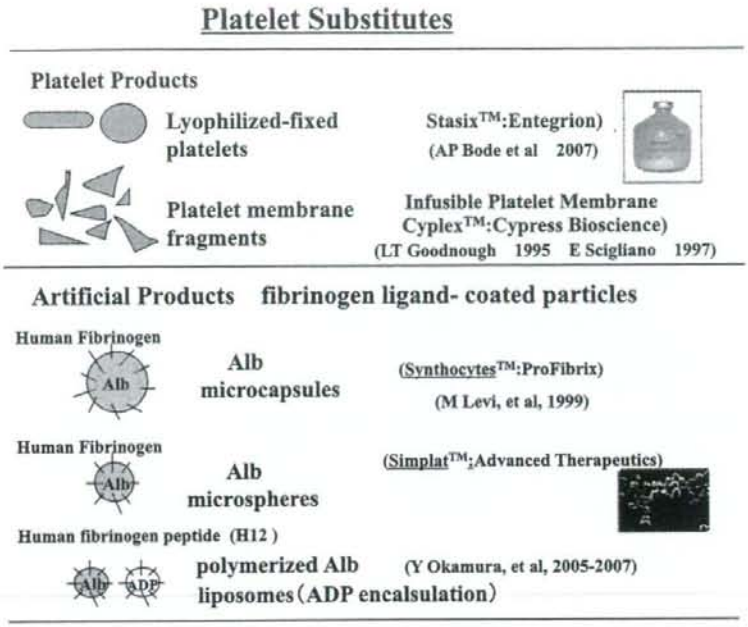

図1　開発された血小板代替物

やSimplat™）は初期臨床研究に供された．

血小板代替物の開発戦略

血小板代替物が具備可能な血小板機能は，#1：止血局所への特異的な集積能力，#2：血小板血栓（血小板凝集）を促進する能力，#3：フィブリン血栓の形成促進能力すなわち凝固活性，であると考えられる．実際，血小板輸血が必要な場合にも患者の血小板が全くなくなることはない．生きた血小板と同等の機能を人工的に創出すことは事実上不可能であり，残存した患者血小板を有効に止血局所で働かせるような機能を最小限保有した製造物が合理的かつ実際的である．一方，安全性の面で重要なのは，その機能は止血局所でのみ特異的に働き，全身的な血栓形成を促すものではけっしてないことである．また，適応に関しての重要なポイントは，出血の予防までを目的とするのか，あるいは単に緊急避難的な止血効果を狙った治療薬とするのかである．出血予防を目的とする場合は，血中での滞留時間をできるだけ長く保つ必要があり，生体適合性を高める目的で，粒子径を可及的に小さくしたり，あるいはポリエチレングリコール鎖による表面修飾（PEG化）を行ったりする工夫が必要である．一方，緊急時の止血薬として使用するならば，血中滞留時間は短くても問題はない．

血小板代替物：各論

前臨床を経て，実際にヒトへの臨床試験まで行き着いたものは数えるほどしかなく，しかも未だにどれも実用化には至っていない．また，そのほとんどがベンチャー企業主導のもとで開発されたもので，したがってそのデータの詳細はほとんど公表されていない．

1）血小板由来産物

凍結乾燥血小板膜断片（IPM：Cyplex™）と

50年近くの試行錯誤の結果開発された固定凍結乾燥血小板（Stasix™）が双璧である[2) 3)]．両者ともその表面のGPIb/IX受容体はインタクトで，それ介したフォンビレブランド因子（VWF）との結合により，止血局所への特異的集積性を有する．また，特徴として，止血局所でその表面を介した凝固因子活性化によるトロンビン生成を助長する働きがある．一方，フィブリノゲノなどと結合して血小板凝集を活性化依存性に惹起するのがGPIIb/IIIa受容体であるが，これらの産物では当然のことながら活性化機構は損なわれており，血小板凝集は起こさない．特にIPMは他に先駆けて臨床試験を行い，フェーズII試験では，5万以下の血小板減少症患者40例のうち27例（65%）で出血症状の改善をきたした[1)]．しかし，その後のフェーズIII試験の後，その理由は公表されないまま開発は中止された．一方，後者は，現在も開発が続けられており，マイルドな条件下でのアルデヒド固定により，血小板の細胞内のシグナル伝達機構の一部は保存され，したがってその表面のGPIb/IX受容体と止血部位に発現したVWFを介した局所集積性を示した後の活性化ステップにより，膜表面の変化を来たして，凝固因子カスケード促進の場を提供すること（凝固活性）で，強力な止血作用を及ぼすとされている[2)]．Stasix™の血中停留時間は極めて短く（半減期：10分），したがって全身性の血栓惹起作用は避けることができるとされ，緊急避難的な（たとえば戦場）止血治療薬として開発が進められている．

2）人工血小板代替物

初期には赤血球が用いられたが，その後は生体適合性に優れたアルブミンとリポソームの2種類が担体（微粒子）として，また認識表面としてヒトフィブリノゲンやその関連ペプチド（RGDなど）などのリガンドを用いたものが主流である[1)]．一方，遺伝子組み換えの血小板接着受容体（GPIbα断片，コラーゲン受容体のGPIa/IIa受容体断片）を認識表面とした人工物もいくつか発表されたが，実用化の面から人工血小板としての検討はそれ以上なされていない[4)]．

（1）アルブミン微粒子

フィブリノゲンやそのRGDペプチドが表面固定された赤血球（Thromboerythrocyteなど）は，フィブリノゲンの受容体であるGPIIb/IIIa複合体を介して活性化血小板と特異的に結合することで血小板凝集を促進して，止血効果を来すことが明らかとなり，赤血球の代わりにアルブミン微粒子を用いたフィブリノゲン結合人工物がいくつか開発された[1)5)]．1995年には，平均径が1.2ミクロンのアルブミン・マイクロスフェアー（Simplat™）が，1999年には，より大型の平均径3.5～4.5ミクロンのアルブミン・マイクロカプセル（Synthocyte™）が報告され，前者はフェーズIII，後者は少なくともフェーズIIまでの臨床試験が行われた[1)6)]．いずれも血液疾患に伴う血小板減少症患者の出血の治療と予防に適用されたが，その結果は公表されておらず，いまだ実用化されていない．2003年には，厚生労働科学研究費の補助により我が国で開発されたアルブミン重合体が報告された．この人工物は認識表面としフィブリノゲンのGPIIb/IIIa複合体に特異的な結合部位であるγ鎖C末端ドデカ配列由来合成ペプチド（^{400}HHLGGAKQAGDV^{411}：H12）を担持させることで，その活性化血小板への特異性を増した．またそのサイズは，0.2ミクロンとより小型で，表面をPEG化することで，その血中滞留時間（半減期：約8時間）を大幅に延ばすことに成功した[7)]．一方，アルブミン・マイクロスフェアーの表面にフィブリノゲンそのものではなくヒトフィブリノゲン親和性合成ペプチドを担持させた人工物（HaemoPlax™）が開発された（http://www.haemostatix.com/）．これは，投与後，血中のフィブリノゲンが表面にコートされて止血効果を来すとされている．いずれの微粒子もその止血作用は，活性化血小板に結合して血小板凝集を増強することで発揮されると考えられ

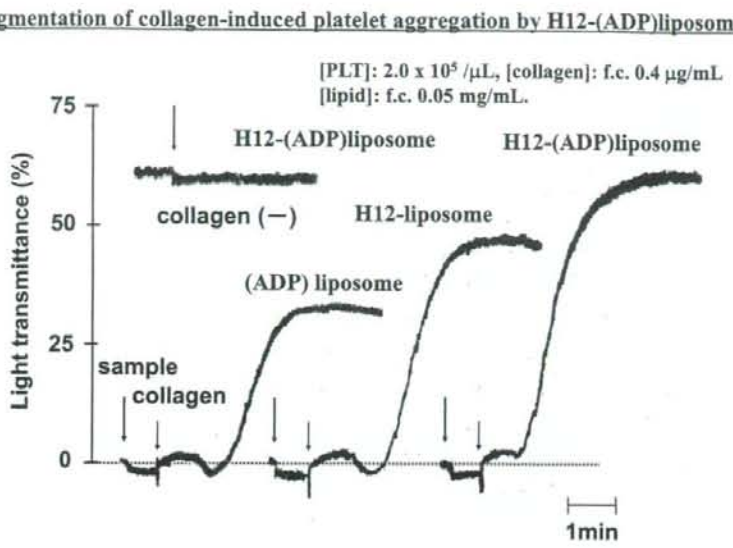

図2　H12結合リポソームのコラーゲン惹起血小板凝集増強作用（ADP内包化の効果）[8]

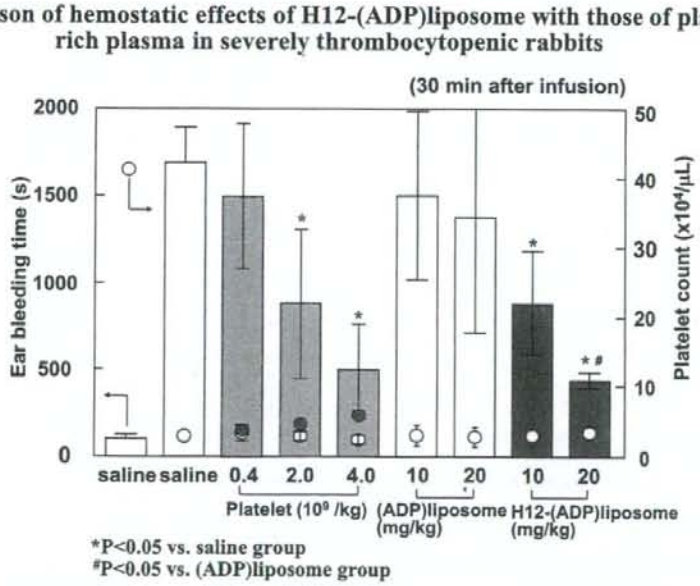

図3　H12結合（ADP）リポソームのウサギ血小板減少症モデルにおける出血時間短縮効果（血小板輸血との比較）[8]

る．したがって，その効果は残存血小板に依存することとなり，血小板数の極めて低い場合にはその止血作用は期待できない可能性がある．

(2) リポソーム

リポソームは生体適合性に優れ，すでに医薬品のDDS担体として実用に供されており，リ

ポソームを担体とした人工血小板代替物がH12結合アルブミン重合体とともに厚生労働科学研究費の補助により開発が進められてきた．実際，H12結合リポソームは *in vitro* でアゴニスト惹起血小板凝集を増強する効果が見られ，ブスルファンによるラット血小板減少症モデルにおいて延長した出血時間を短縮する効果が認められた．しかし，H12結合アルブミン重合体と比較するとその効果は弱かった．これは多分，アルブミン重合体で予想される局所充填効果がリポソームでは期待できないためかもしれない．そこで，リポソームのDDS機能を用い，生理的な血小板アゴニストであるアデノシン2リン酸（ADP）を内包化したところ（H12-(ADP) リポソーム），より強力な *in vitro*（アゴニスト惹起血小板凝集増強作用），*in vivo*（血小板減少症動物モデルでの出血時間短縮作用）機能を付加することに成功した[8]（**図2,3**）．H12-(ADP) リポソームは止血局所に特異的に集積すること，内包化したADPの放出は血小板凝集に依存していること，したがって動物モデルでは明らかな血小板の活性化や凝固系の亢進は全身的には認められなかった．ウサギ血小板減少症モデルでは，血小板輸血に匹敵した効果的な出血時間短縮効果が認められ，完全な人工物として開発の進展が期待されている．

おわりに

血小板代替物の開発の歴史は古いにもかかわらず未だに実用化に至っていない．前臨床では明らかな血小板代替機能が認められても，実際の臨床試験をクリアーできていない．しかし，開発は続けられており，その方向性は，米国での軍事目的（緊急避難的な止血薬）での凍結乾燥固定血小板，そして，一般の医療における出血の予防や治療を目的とした人工血小板微粒子（アルブミン，リポソーム）であり，いずれも臨床試験を想定した段階にあると思われる．

謝辞：本総説で紹介した研究の一部は平成20年度厚生労働科学研究費助成，政策創薬総合研究分野「臨床応用可能な人工血小板としてのH12結合微粒子の *in vivo* 評価」（H18-創薬-一般-026；主任研究者：半田誠）によって行われた．

文　献

1) Blajchman MA : Substitutes and alternatives to platelet transfusions in thrombocytopenic patients. J Thromb Haemost **1** : 1637-1641, 2003.
2) Graham SS, Gonchoroff NJ, Miller JL : Infusible platelet membranes retain partial functionality of the platelet GPIb/IX/V receptor complex. Am J Clin Pathol. **115** : 144-151, 2001.
3) Bode AP, Fischer TH. Lyophilized platelets : fifty years in the making. Artif Cells Blood Substit Immobil Biotechnol **35** : 125-133, 2007.
4) Nishiya T, Kainoh M, Murata M, Handa M, Ikeda Y : Reconstitution of adhesive properties of human platelets in liposomes carrying both recombinant glycoproteins Ia/IIa and Ibalpha under flow conditions : specific synergy of receptor-ligand interactions. Blood. **100** : 136-141, 2002.
5) Coller BS, Springer KT, Beer JH, Mohandas N, Scudder LE, Norton KJ, West SM : Thromboerythrocytes. In vitro studies of a potential autologous, semi-artificial alternative to platelet transfusions.J Clin Invest. **89** : 546-555, 1992.
6) Levi M, Friederich PW, Middleton S, de Groot PG, Wu YP, Harris R, Biemond BJ, Heijnen HF, Levin J, ten Cate JW : Fibrinogen-coated albumin microcapsules reduce bleeding in severely thrombocytopenic rabbits.Nat Med. **5** : 107-111, 1999.
7) Okamura Y, Fujie T, Maruyama H, Handa M, Ikeda Y, Takeoka S. Prolonged hemostatic ability of poly (ethylene glycol)-modified polymerized albumin particles carrying fibrinogen γ-chain dodecapeptide. Transfusion **47** : 1254-1262, 2007.
8) Okamura Y, Takeoka S, Eto K, Maekawa I, Fujie T, Maruyama H, Ikeda Y, Handa M : Development of fibrinogen γ-chain peptide-coated, adenosine diphosphate-encapsulated liposomes as a synthetic platelet substitute. J Thromb Haemost (in press).

New Technology

人工血小板の開発

Development of Artificial Platelets

岡村 陽介[1,2]・武岡 真司[1]・半田 誠[2]・池田 康夫[3]

Key Words: Artificial platelet, polymerized albumin particle, phospholipid vesicle, rGPIbα, rGPIa/IIa, fibrinogen γ-chain dodecapeptide (H12)

Abstract

血小板は，血液凝固系と連動した巧妙な止血機構を有しており，これらすべてを具備した人工系の構築は不可能といっても過言ではない。我々は，血小板が出血部位において認識して粘着，凝集する分子機構に着目し，その主要な分子(GPIbα，GPIa/IIa，フィブリノーゲン由来アミノ酸配列(H12)など)を担持させた静注可能な人工微粒子(アルブミン重合体やリン脂質小胞体)を設計し，特異的に出血部位へ集積させ，活性化血小板と共に充填させることにより止血効果を期待した。本報ではその評価結果を報告する。

■はじめに

医療の進歩に伴い，癌・造血器腫瘍などの化学治療や放射線治療が年々増加する一方で，その副作用により血小板減少患者が増大している。血小板輸血は，化学治療，放射線治療，あるいは外科手術において不可欠な補助治療法として重要な位置を占めており，その供給量は年々増加し続け，平成11年以降は一定推移を保っている[1]。しかし，血小板製剤の保存期間は室温で4日間と非常に短いため，慢性的な供給不足に加えて緊急時の供給体制は整っていない。

更に，核酸増幅検査(NAT)の導入により血液製剤の安全性は著しく向上したものの，未だにウィルス感染などのリスクは完全には払拭されていない。従って，人工血小板の開発並びに臨床応用は，21世紀に於ける医療において当然目指すべき方向と思われる。

■止血機序と人工血小板の設計

止血の初期段階は，血管損傷部位に露出している血管内皮下組織への血小板の粘着と凝集である。高血流状態では，血小板膜糖蛋白質Ib(GPIb)がフォンビレブランド因子(VWF)を介したコラーゲンとの相互作用によって血小板の接着(ローリング)が起こる。続いて，低血流状態でコラーゲンの受容体蛋白質であるGPIa/IIaやGPVIがコラーゲンと直接結合して強固な粘着が起こる。接着，粘着の刺激が細胞内シグナルとして伝達されGPIIb/IIIaの高次構造が変化し(活性化)，血漿蛋白質であるフィブリノーゲンやVWFを介した血小板凝集が起こる。同時に，血小板内の濃染顆粒が開放小管系と膜融合してアデノシン5'-二リン酸(ADP)，Ca^{2+}，セロトニンが放出され，血小板間，あるいは白血球をも巻き込んだネットワークを形成して血小板凝集(一次止血)を促す。最後にトロンボキサンA_2の放出や血小板表面が凝固系の活性に必要な場(ホスファチジルセリン)として提供され，凝固因子カスケード反応が活性化されてフィブリン塊(血餅)となって止血(二次止血)が完了する。

このように血小板による止血には，巧妙に制御された多段階の反応が連動しているため，この機能を全て模倣した人工系の構築は不可能である。我々は，血小板が出血部位を認識して粘着，凝集する分子機構に着目し，血管損傷部位や血小板表面を認識できる分子を微粒子表面に担持させれば，これが出血部位へ特異的に集積して血栓形成を誘

Yosuke Okamura[1,2], Shinji Takeoka[1], Makoto Handa[2], and Yasuo Ikeda[3]
[1] 早稲田大学先進理工学部生命医科学科[2] 慶應義塾大学医学部輸血・細胞療法部[3] 慶應義塾大学医学部内科
[1] Department of Life Science and Medical Bioscience, School of Advanced Science and Engineering, Waseda University.[2] Department of Transfusion Medicine & Cell Therapy, School of Medicine, Keio University.
[3] Department of Internal Medicine, School of Medicine, Keio University.

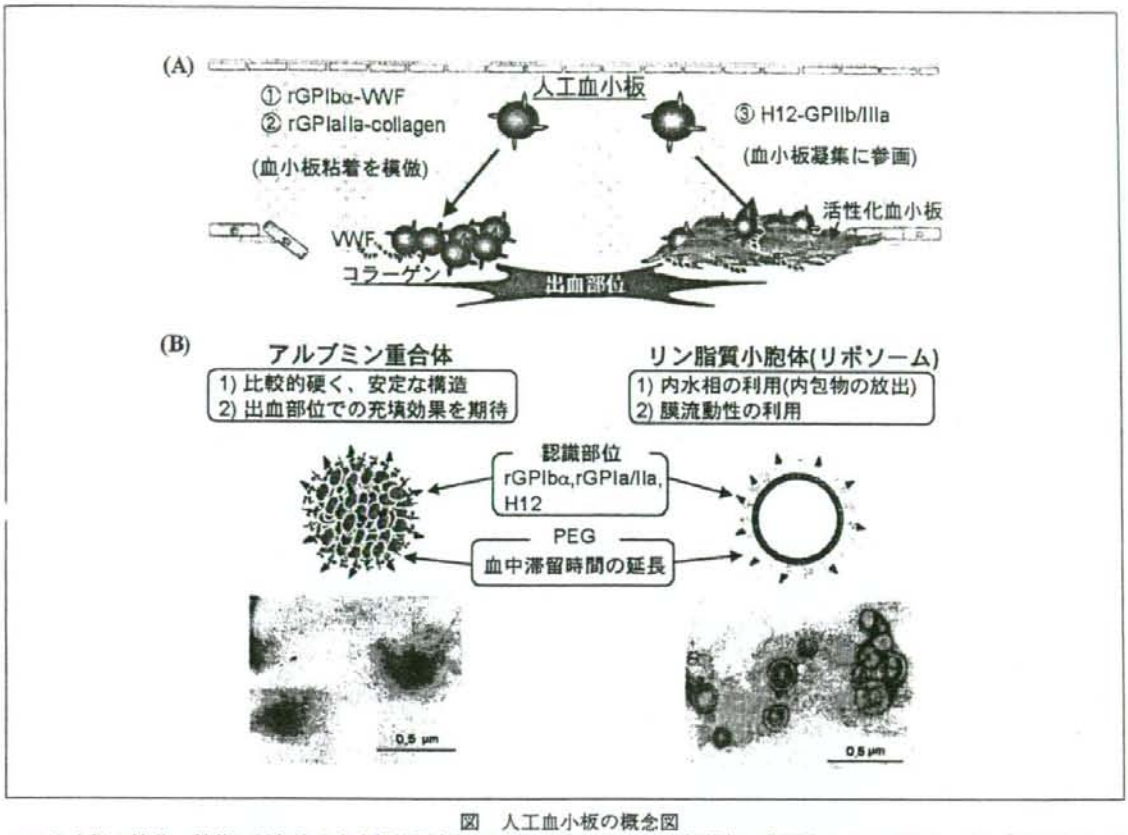

図　人工血小板の概念図
(A) 血小板の接着，粘着に関与する血小板膜蛋白質rGPIbα, rGPIa/IIa，血小板凝集に参画するフィブリノーゲン由来ドデカペプチド(H12)を微粒子表面に結合させることで出血部位へ特異的に集積させ，出血部位の充填効果が期待できる。
(B) 人工血小板用の担体として開発したアルブミン重合体とリン脂質小胞体の特徴と電子顕微鏡像。

導する起点となり，出血部位を充填して止血効果が期待できるとの発想から，極めて単純な人工血小板の設計に結びつけた（図(A)）。具体的には，静注可能な遺伝子組換えヒト血清アルブミン(rHSA)の重合体やリン脂質小胞体(リボソーム)を微粒子として利用し，出血部位を認識させるために血小板膜糖蛋白質の一部の遺伝子組換え蛋白質(rGPIbα，rGPIa/IIa)やフィブリノーゲンγ鎖C末端アミノ酸配列(HHLGGAKQAGDV: H12)を担持させた系を構築して*in vitro*，*in vivo*評価を行っている。

■微粒子の製造方法と機能評価

我々は，rHSAを単量体とし，そのpHと温度の制御のみでジスルフィド重合させるクリーンかつ簡便なアルブミン重合体の調製法を確立している[2]。重合度の制御によりナノからマイクロスケールの粒径制御が可能であり，アルブミン重合体は内部が充填された無定形な形態をとっている（図(B)）。他方，リン脂質を水中に分散させると自発的に集合して多重層小胞体が構築される。これを孔径の異なるメンブレンに順次透過させると，粒子径と膜層数の制御が可能となる。さらに，小胞体表面へ種々の蛋白質を担持させて特定部位への指向性，集積性が期待できる（図(B)）。

小胞体やアルブミン重合体の表面にrGPIbαやrGPIa/IIaを結合させると，血小板の接着(ローリング)，粘着現象が再現できる[3]。興味深いことにそのローリング速度は，小胞体を構成する二分子膜の柔軟性と相関しており，“柔らかい”小胞体ではローリング速度は低下し，“硬い”小胞体では上昇した。これは“柔らかい”小胞体は変形しやすくVWF基板と小胞体間の接触面積が増大したために

ローリング速度が低下したためと考えられる。ところが，アルブミン重合体ではVWF表面をローリングせずに粘着する。従って，ローリングには流動性のある膜構造が必要と思われた。

他方，アルブミン重合体や小胞体にフィブリノーゲンγ鎖C末端ドデカペプチド(HHLGGAKQAGDV, H12)を結合させると，血小板凝集促進機能が発現する[4, 5]。具体的には，血小板減少モデル血液(2.0×10^4 /μL，正常の10分の1)にH12結合アルブミン重合体を添加し，コラーゲン基板に対する血小板の粘着挙動を流動下で観察したところ，その未添加系と比較して血小板の粘着を約2倍も増大させた。さらに，抗がん剤(ブスルファン)をWister系雄性ラットに20 mg/kgにて投与すると，その副作用によって，投与10日後に血小板数のみが正常の5分の1まで再現性よく減少した[4]。血小板減少症モデルラットの尾先端から1cmの箇所をクイックヒール®にて切傷後，生理食塩水に浸して出血時間を測定すると，再現性良く計測できた(608±152秒，正常ラット：178±56秒)。そこで，H12結合アルブミン重合体を投与すると出血時間が投与量依存的に有意に短縮された(288±120秒)[4]。

また，血中滞留時間の延長を目的としてアルブミン重合体の表面をポリエチレングリコール鎖にて修飾し，その末端の一部にH12を結合した系では，投与6時間後でもその止血効果が持続することも確認できている。また，担体を小胞体に置き換えても，同様の止血効果が得られている[5]。しかし，この両者を同一粒子数を投与した群同士で比較した場合，アルブミン重合体の方がその効果は優れているようである。これは，アルブミン重合体は内部が充填されているため，出血部位の充填効果が高いためと推測できる。しかし，小胞体ならば内水相に血小板の活性化や凝固系を誘導する因子を内包可能であり，出血部位に集積した小胞体がこれらを放出することにより，より効果的に出血時間を短縮する系の構築も可能になりつつある(未発表データ)。

■今後の展開と課題

血小板減少動物モデルを用いた止血効果に関する知見も次々に集積され，我々の人工血小板の設計方針の正当性が立証でき，人工血小板の実用化の可能性が見えてきた。今後は，臨床試験に向けてその適応を明確にした上で，より大型動物(ウサギ，霊長類)を用いた効能試験や安全性試験(血液生化学試験，毒性試験)を行う必要がある。将来，バイオテクノロジーやオプトエレクトロニクスの進歩により血小板の動的機能に関する多くの情報が短期間に蓄積され，同時に遺伝子組換え蛋白質の大量製造や担体の製剤化技術の飛躍が期待できるため，我々の研究成果は人工血小板の開発のみならずDrug Delivery Systemの基盤技術の発展にも繋がるものと期待される。

文　献

1) 日本赤十字社ホームページ　http://www.jrc.or.jp/active/blood/index.html.
2) Takeoka S *et al.*: Biomacromolecules. 1: 427-462, 2000.
3) Takeoka S *et al.*: Biochem. Biophys. Res. Commun. 296: 765-770, 2002.
4) Okamura Y *et al.*: Transfusion. 45: 1221-1228, 2005.
5) Okamura Y *et al.*: Bioconjugate Chem. 16: 1589-1596, 2005.

News (学会情報)

第112回　日本眼科学会総会

テーマ：そして未来へ。
会　期：2008年4月17日（木）～20日（日）
会　場：パシフィコ横浜　http://www.pacifico.co.jp/
招待講演　4月19日（土）10:50～11:50　第1会場（メインホール）
2）バイオマテリアルと生体組織工学とを駆使した先端医療の最前線
座長：吉村　長久　京都大学
演者：田畑　泰彦　京都大学・再生医科学研究所生体組織工学研究部門　生体材料学分野
●第112回 日本眼科学会総会 運営事務局（株式会社コングレ内）
〒102-8481 東京都千代田区麹町5-1 弘済会館ビル　TEL：03-5216-5551　FAX：03-5216-5552

Prolonged hemostatic ability of polyethylene glycol–modified polymerized albumin particles carrying fibrinogen γ-chain dodecapeptide

Yosuke Okamura, Toshinori Fujie, Hitomi Maruyama, Makoto Handa, Yasuo Ikeda, and Shinji Takeoka

BACKGROUND: Second-generation platelet (PLT) substitutes for treatment of bleeding were studied and the focus was on a dodecapeptide, HHLGGAKQAGDV (H12), which is a fibrinogen γ-chain carboxy-terminal sequence (γ 400-411) and exists only in a fibrinogen domain.

STUDY DESIGN AND METHODS: H12 was conjugated to the surface of polymerized albumin particles (polyAlb) modified with polyethylene glycol (PEG) chains to produce biocompatible particles (H12-PEG-polyAlb) that had prolonged blood circulation $t_{1/2}$ and were more stable in vitro and in vivo compared with H12-polyAlb (not modified with PEG). H12-PEG-polyAlb was administered intravenously into thrombocytopenic rats and the $t_{1/2}$ of the particles and the tail bleeding time were measured to evaluate the prolongation in the hemostatic effect.

RESULTS: H12-PEG-polyAlb particles modified with PEG prolonged the $t_{1/2}$ and maintained specific binding ability to activated PLTs. The particles dose dependently shortened the tail bleeding time of thrombocytopenic rats 6 hours after injection.

CONCLUSION: H12-PEG-polyAlb may be a suitable candidate for treatment of bleeding into thrombocytopenic patients as an alternative to PLT concentrate transfusion.

Platelet (PLT) transfusion plays an important role in the supportive therapy of thrombocytopenia caused by cancer or hematologic malignancies or in the perioperative period. The shortage of PLT concentrates, however, has always been a serious issue because of the short storage life (72 hr in Japan), insufficient donation, and the greater rate of demand than

ABBREVIATIONS: GP = glycoprotein; H12-PEG-polyAlb = polymerized albumin particles carrying H12 at the end of the polyethylene glycol chains; MALPEG-NHS = α-(3-[3-maleimido-1-oxopropyl]amino) propyl-ω-succinimidyl carboxypentyloxy polyethylene glycol; mPEG-NHS = α-methoxy-ω-succinimidyl carboxypentyloxy monofunctional PEG; PGE_1 = prostaglandin E_1; polyAlb = polymerized albumin particles; rHSA = recombinant human serum albumin.

From the Department of Applied Chemistry, Graduate School of Science and Engineering, Waseda University, Tokyo; and the Department of Internal Medicine and the Department of Transfusion Medicine & Cell Therapy, School of Medicine, Keio University, Tokyo, Japan.

Address reprint requests to: Shinji Takeoka, Department of Applied Chemistry, Graduate School of Science and Engineering, Waseda University, Tokyo 169-8555, Japan; e-mail: takeoka@waseda.jp.

This work was supported in part by Health and Labor Sciences Research Grants (Research on Pharmaceutical and Medical Safety, ST, MH, and YI); Ministry of Health, Labor and Welfare, Japan, and grants-in-aid from the JSPS, Japan (No. 15300171, ST); Ministry of Education, Culture, Sports, Science and Technology (Leading Project for Biosimulation, MH); and 21COE "Practical Nano-Chemistry" and "Consolidated Research Institute for Advanced Science and Medical Care" from MEXT (ST), Japan. YO was the recipient of a Research Fellowship from the JSPS for Young Scientists.

Received for publication October 6, 2006; revision received December 25, 2006, and accepted January 2, 2007.

doi: 10.1111/j.1537-2995.2007.01265.x

TRANSFUSION 2007;47:1254-1262.

supply. Furthermore, the risk of viral and bacterial infections associated with transfusion is also a serious issue. For these reasons, a number of trials have been conducted to develop PLT substitutes (artificial PLTs) reproducing PLT functions such as tethering and adhesion, or enhancing the hemostatic ability,[1] such as infusible PLT membranes,[2] solubilized PLT membrane protein–conjugated liposomes (plateletsome),[3] fibrinogen-bonded red blood cells (RBCs),[4] fibrinogen-coated albumin microcapsules (synthocyte),[5] liposomes bearing fibrinogen,[6] and arginine-glycine-asparaginic acid (RGD) peptide-bound RBCs (thromboerythrocytes).[7] These PLT substitutes consist of materials derived from blood components.

Glycoprotein (GP) IIb/IIIa, which exists on the PLT membrane, changes from an inactive form to an active form when PLTs adhere to a collagen-immobilized surface.[8-10] The activated GPIIb/IIIa acts as a receptor for fibrinogen and von Willebrand factor,[11-13] followed by PLT aggregation.[14,15] This is because fibrinogen contains three putative binding sites to GPIIb/IIIa, namely, a tetrapeptide containing an RGD sequence, for example, RGDF and RGDS at α95-98 and α572-575, respectively, and a dodecapeptide (HHLGGAKQAGDV, H12) at a α-chain carboxy-terminal segment (α400-411).[16]

To prepare the PLT substitutes enhancing the hemostatic ability, we also conjugated fibrinogen[17] to biocompatible carriers such as polymerized albumin particles (polyAlb)[18,19] and phospholipid vesicles (liposomes).[20-24] These fibrinogen conjugates were shown to facilitate PLT aggregation on an activated PLT-immobilized surface in vitro by recruitment of the flowing PLTs in the aggregates after their attachment.[17] Fibrinogen isolated from human plasma, however, is not stable[17] and tends to precipitate at 4°C within a few hours.[25]

Therefore, we focused on a stable dodecapeptide (H12) instead of fibrinogen.[16,26-29] Based on our results obtained from the flow cytometric analyses of PLT agglutination, the H12 conjugates showed minimal interaction with nonactivated PLTs compared with RGD conjugates.[30] Furthermore, the H12-conjugated polyAlb enhanced the in vitro thrombus formation on a collagen-immobilized plate when exposed to the flowing thrombocytopenia imitation blood.[31] When we measured the tail bleeding time at 5 minutes after the injection of the H12-polyAlb, we found a dose-dependent reduction in the bleeding time. The H12-polyAlb was of limited use, however, because the $t_{1/2}$ of the H12-polyAlb was extremely short (approximately 10 min).[31]

Polyethylene glycol (PEG) modification on the surface of carriers such as phospholipid vesicles or biocompatible polymeric particles has been widely used to prolong the $t_{1/2}$ or to stabilize their dispersion states.[32-35] We previously reported that PEG modification of the vesicles was effective in preventing intervesicular access and aggregation with a capillary viscosimeter and an optical microscope. Also, subcutaneous microvascular studies showed that the PEG conjugates significantly improved microcirculation (flow rate, functional capillary density, and vessel diameter).[24,32,33]

Our purpose was to produce a PLT substitute enhancing the hemostatic ability for the treatment of bleeding. In this study, we prepared polyAlb particles carrying H12 at the end of the PEG chains (H12-PEG-polyAlb) to prolong their $t_{1/2}$ and to enhance their stability in vitro and in vivo. The H12-PEG-polyAlb particles were intravenously administered into thrombocytopenic rats, and the tail bleeding time and the blood circulation $t_{1/2}$ were measured for evaluation of the increased hemostatic effect.

MATERIALS AND METHODS

Reagents

Fibrinogen γ-chain dodecapeptide (C-HHLGGAKQAGDV, H12) was synthesized with a solid-phase synthesizer by BEX (Tokyo, Japan). Two kinds of PEG, namely, α-(3-[3-maleimido-1-oxopropyl]amino) propyl-ω-succinimidyl carboxypentyloxy PEG (MALPEG-NHS, MW 5.0 kDa), and α-methoxy-ω-succinimidyl carboxypentyloxy monofunctional PEG (mPEG-NHS, MW 5.0 kDa), were purchased from NOF (Tokyo, Japan). Prostaglandin E_1 (PGE_1), busulfan, and PEG (mean molecular weight, 400 Da) were obtained from Sigma-Aldrich (St Louis, MO). PAC-1 and mouse immunoglobulin M (IgM) were obtained from Becton Dickinson (San Jose, CA). Fluorescein-4-isothiocyanate (FITC) was purchased from Dojindo Laboratories (Kumamoto, Japan). Recombinant human serum albumin (rHSA) was donated by Mitsubishi Pharma (Osaka, Japan).

Preparation of polyAlb

A solution of rHSA (250 mg/mL) was dialyzed against distilled water for 6 hours at 4°C to remove stabilizers such as *N*-acetyl-D,L-tryptophan and sodium caproate. The rHSA solution (200 mL) was diluted with saline to 10 mg per mL and the pH was adjusted to 10.7 (at room temperature) by titration with 0.1 N NaOH (6.4 mL). The solution was heated at 80°C for 10 minutes and rapidly cooled in an ice bath and then brought to room temperature The pH was adjusted to 6.1 at room temperature by dropwise addition of 0.1 N HCl (7.2 mL). The solution was then stirred at 40°C for approximately 120 minutes until the turbidity reached 0.4 ± 0.02. Excess iodoacetamide (25 mg) was added to terminate polymerization, and the solution was dialyzed against phosphate-buffered saline (PBS, pH 7.4) at 4°C for 24 hours. The polyAlb suspension (213 mL) was centrifuged and washed with PBS (30,000 × g, 10 min, 4°C) to separate the rHSA oligomers. The resultant preparation was the purified polyAlb ([rHSA] = 20 mg/mL, 30 mL). A

mean particle diameter was determined by a dynamic scattering method (Coulter N4 Plus submicron particle sizer, Beckman-Coulter, Miami, FL).

PEG modification with the surface of polyAlb carrying H12

A solution of MALPEG-NHS in dimethyl sulfoxide (DMSO; 10 mmol/L, 284 μL) was added to the polyAlb suspension (20 mg/mL [300 μmol/L], 30 mL), and the suspension was stirred for 20 minutes at room temperature. Different volumes of a 25 mmol per L solution of mPEG-NHS in DMSO (0, 284, 1136, 1704, and 2840 μL) were added to aliquots of this suspension, and the suspensions were stirred for 20 minutes at room temperature. The unreacted reagents and the by-products were separated by repeated centrifugation and washing with PBS (30,000 × *g*, 10 min, 4°C) and MALPEG- and mPEG-modified polyAlb ((MALPEG)(mPEG)polyAlb) were collected. A suspension of (MALPEG)(mPEG)polyAlb (20 mg/mL, 20 mL) was mixed with a solution of H12 (100 mmol/L, 19 μL) and allowed to react at room temperature for 12 hours. A small molar excess of cysteine over MALPEG was added to the suspension, and the unreacted reagents were removed by repeated centrifugation and washing with PBS (30,000 × *g*, 10 min, 4°C) to obtain the purified (MALPEG)(mPEG) polyAlb carrying H12 (H12-PEG-polyAlb, 10 mg/mL, 30 mL). Similarly, FITC-labeled H12-PEG-polyAlb was prepared as follows: a solution of FITC was added to the (MALPEG)(mPEG)polyAlb suspension before H12 conjugation and stirred for 20 minutes at room temperature. The unreacted FITC and the by-products were separated at the same time during separation of unreacted PEG.

The concentrations of the MALPEG, mPEG, and H12 conjugated to the surface of polyAlb were determined by the quantification of each unreacted reagent with high-pressure liquid chromatography on a TSK-GEL G3000PW$_{XL}$ column (7.8 mm o.d. × 300 mm hr with a mobile phase of 36% acetonitrile and 0.1% trifluoroacetic acid at 1 mL/min). Unreacted reagents were detected with a reflective index detector. H12-polyAlb particles to which H12 was directly conjugated were prepared with a cross-linker; *N*-succinimidyl 3-(2-pyridyldithio) propionate as described previously.[31]

Flow cytometric analyses

Blood withdrawn from healthy volunteers was mixed with 10 percent volume of 3.8 percent (wt/vol) sodium citrate. PLT-rich plasma was prepared by centrifugation (100 × *g*, 15 min, 22°C). PLT-rich plasma was mixed with a 15 percent (vol/vol) acid-citrate-dextrose (ACD) solution composed of 2.2 percent (wt/vol) sodium citrate, 0.8 percent (wt/vol) citric acid, and 2.2 percent (wt/vol) glucose (ACD) containing 1 μmol per L PGE_1. The suspension was centrifuged (2200 × *g*, 10 min, 22°C), and the plasma was replaced with a Ringer's-citrate-dextrose solution (composition, 0.76% [wt/vol] citric acid, 0.090% [wt/vol] glucose, 0.043% [wt/vol] $MgCl_2$, 0.038% [wt/vol] KCl, 0.60% [wt/vol] NaCl, pH 6.5) containing 1 μmol per L PGE_1. After the pellets were resuspended in the Ringer's-citrate-dextrose solution, the suspension was centrifuged (2200 × *g*, 10 min, 22°C), and the concentrated PLTs were resuspended at 100×10^3 per μL in a Hepes-Tyrode buffer (pH 7.4). The PLT counts were determined with an automated hematology analyzer (K-4500, Sysmex, Kobe, Japan).

The suspension of the FITC-labeled H12-PEG-polyAlb (14 mg/mL, 20 μL) was added to the PLT suspension ([PLT] = 100×10^3/μL, 50 μL) in the presence or absence of PAC-1 (approx. 0.5 μg). Thrombin (final concentration, 3 U/mL) was added to the suspension to activate the PLTs at 37°C for 10 minutes before fixing with formaldehyde (final concentration, 1.5% [vol/vol]). We carried out the same experiments for control PEG-polyAlb, H12-polyAlb, and polyAlb. The PLTs were gated to their characteristic forward versus side scatter, and 20,000 PLTs were analyzed with a flow cytometer (FACSCalibur, Nihon Becton Dickinson, Tokyo, Japan). The PLTs binding with the H12-PEG-polyAlb was quantified as a fraction of the fluorescent-positive PLTs. Each experiment was performed at least three times.

Measurement of tail bleeding time and $t_{1/2}$ of H12-PEG-polyAlb with thrombocytopenic rats

All animal studies were approved by the Animal Subject Committee of Keio University, School of Medicine, and performed according to NIH guidelines for the care and use of laboratory animals. Busulfan-induced thrombocytopenic rats were prepared as described previously.[31] A busulfan solution was prepared at a final concentration of 5 mg per mL in PEG (mean molecular weight, 400).[31] Male Wistar rats (230-250 g, CLEA Japan, Tokyo, Japan) were anesthetized with diethyl ether and injected on Days 0 and 3 with 10 mg per kg on each dosing day to produce a total dosage of 20 mg per kg busulfan. On Day 10, thrombocytopenic rats were anesthetized with sevofrane, and the sample suspension was infused into the tail vein. The samples were H12-PEG-polyAlb and PEG-polyAlb at a dose of 4 mL per kg; saline was used to obtain the control value. Several hours after administration, a 2.5-mm (length) × 1.0-mm (depth) template-guided incision (Quikheel, Becton-Dickinson) was made 1 cm from the tip of the tail. A tail was immersed in a 50-mL cylinder of saline, and the time taken for bleeding to stop was measured.

The blood circulation $t_{1/2}$ was measured from the clearance curve as follows: FITC-labeled H12-PEG-polyAlb suspension was infused into the tail vein at a dose

of 40 mg per kg (equivalent rHSA concentration). After this, 400 µL of blood was collected from the tail vein of the rats at time intervals with a 25-gauge needle and centrifuged (2200 × *g*, 10 min, 22°C), and 200 µL of plasma containing the polyAlb was collected. The plasma was mixed with a solution of 0.1 N NaOH and incubated at room temperature for 20 min to dissolve H12-PEG-polyAlb. The fluorescent intensity was then measured (E_x = 495 nm, E_m = 510 nm), and the $t_{1/2}$ was calculated with a spectrofluorometer (FP-750, JASCO, Tokyo, Japan).

Statistical analyses

Significance of data for H12-PEG-polyAlb group versus PEG-polyAlb and saline groups was tested with Tukey-Kramer tests (Fig. 3). Significance of data for H12-PEG-polyAlb group versus saline group was tested with a t test (Fig. 4). A p value of less than 0.05 was considered to be significant. Statistical analyses were performed with computer software (StatView, SAS Institute, Cary, NC).

RESULTS

Characterization of H12-PEG-polyAlb

We selected two kinds of PEG reagents; the minimum amount of bifunctional PEG (MALPEG) was used to chemically bond H12 having a mercapto group at the C-terminus, whereas mPEG was used to stabilize dispersion states of polyAlb and do not react with H12. We modified the surface of polyAlb (diameter of 200 ± 80 nm) with MALPEG to the particles. The number of molecules of MALPEG that chemically bound with one polyAlb particle was estimated to approximately 12×10^3 molecules. When the concentration of mPEG added to the MALPEG-polyAlb was 0.78, 3.1, 4.7, and 7.8 mol per mol (mole equivalent of rHSA concentration), the amount of reacted mPEG was found to be 0.35, 0.94, 1.2, and 1.2 mol per mol, respectively. The reaction was saturated at 1.2 mol per mol when the ratio of mPEG to polyAlb was 4.7 mol per mol (Fig. 1). The number of molecules of mPEG attached to one MALPEG-polyAlb particle was estimated to be approximately 18×10^3, 48×10^3, 61×10^3, and 61×10^3 molecules, respectively. The endotoxin concentration in the suspension of H12-PEG-polyAlb was below 0.25 EU per mL.

$T_{1/2}$ of H12-PEG-polyAlb

When we administrated FITC-labeled PEG-polyAlb with various numbers of mPEG modification as described above into thrombocytopenic rats, the $t_{1/2}$ of the particles significantly increased with increasing amount of bound mPEG (Fig. 1). Especially in the case of PEG-polyAlb particles with maximum mPEG modification (61×10^3 molecules), the $t_{1/2}$ of the PEG-polyAlb was estimated to be approximately 188 minutes from the clearance curve, whereas that of the bare unmodified polyAlb was estimated to be approximately 10 minutes (data not shown). Thus, we succeeded in prolonging the $t_{1/2}$ of the polyAlb almost 19-fold by PEG modification.

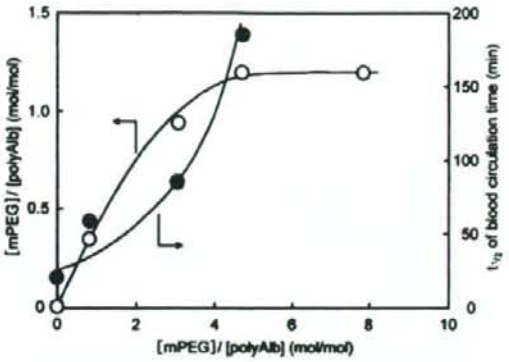

Fig. 1. Correlation of the amount of mPEG conjugated to the polyAlb (○) with blood circulation $t_{1/2}$ (●).

Flow cytometric analyses

When the FITC-labeled H12-PEG-polyAlb was added to the thrombin-stimulated PLT suspension, 86.8 ± 2.2 percent of the PLTs were fluorescently labeled (Fig. 2). In the case of nonstimulated PLTs, the ratio was 1.4 ± 0.3 percent. In the presence of PAC-1, which recognizes an epitope on the GPIIb/IIIa complex of activated PLTs at or near the PLT fibrinogen receptor,[36] the binding of H12-PEG-polyAlb to the stimulated PLTs was significantly inhibited and only 7.3 ± 0.9 percent were fluorescently labeled. The binding was not inhibited in the presence of IgM, which is an isotype-matched negative control immunoglobulin for PAC-1; in this case, 87.0 ± 3.7 percent of the PLTs were fluorescently labeled. The control PEG-polyAlb did not bind to stimulated PLTs. In the case of the H12-polyAlb (not modified with PEG), the ratio of fluorescent-positive PLTs was 91.1 ± 7.9 percent and almost equal to that found with H12-PEG-polyAlb, whereas the bare polyAlb did not show appreciable binding (1.7 ± 0.5%).

Hemostatic effects at 3 hours after H12-PEG-polyAlb administration

The tail bleeding times of the normal rats (PLT count, $810 \times 10^3 \pm 80 \times 10^3$/µL) and the thrombocytopenic rats (PLT count, $190 \times 10^3 \pm 20 \times 10^3$/µL) at 3 hours after the intravenous (IV) administration of saline were 202 ± 51 and 712 ± 131 seconds, respectively (Fig. 3). The bleeding

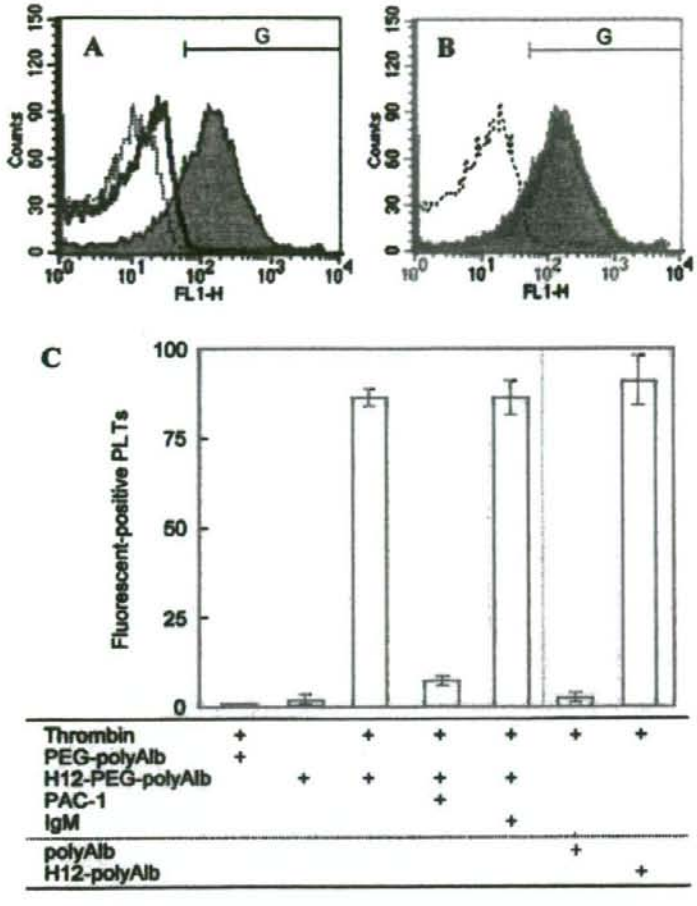

Fig. 2. Specific interactions of H12-PEG-polyAlb with thrombin-stimulated PLTs with flow cytometry. (A) The solid histogram represents thrombin-stimulated PLTs stained with FITC-labeled H12-PEG-polyAlb, the dotted histogram represents thrombin-stimulated PLTs stained with FITC-labeled control PEG-polyAlb, and the open histogram represents thrombin-stimulated PLTs stained with FITC-labeled H12-PEG-polyAlb in the presence of PAC-1. (B) The solid histogram represents thrombin-stimulated PLTs stained with FITC-labeled H12-PEG-polyAlb, the open histogram represents thrombin-stimulated PLTs stained with FITC-labeled H12-polyAlb, and the dotted histogram represents thrombin-stimulated PLTs stained with FITC-labeled control polyAlb. (C) The bar graph form was summarized in triplicate and the percentage fluorescent positive PLTs were quantified as a fraction "G" as shown in A and B.

time of the thrombocytopenic rats was approximately 3.5 times longer than that of the normal rats, suggesting that it was possible to evaluate the hemostatic effect of the H12-PEG-polyAlb in vivo with thrombocytopenic rats.

The bleeding times of the thrombocytopenic rats at 3 hours after the IV administration of the H12-polyAlb or the control polyAlb at a dose of 40 mg per kg were 590 ± 201 and 700 ± 73 seconds, respectively, and the bleeding time was almost comparable to that obtained with the control rats injected with saline. IV administration of the H12-PEG-polyAlb at a dose of 4 mg per kg did not reduce the bleeding time to 626 ± 158 seconds. For the same dose, the bleeding time of the control PEG-polyAlb group was 696 ± 108 seconds. At doses of 20 and 40 mg per kg, there was a dose-dependent reduction in the bleeding time of H12-PEG-polyAlb (Fig. 3); the bleeding times were reduced to 594 ± 184 and 330 ± 73 seconds, respectively. In comparison, the bleeding times of the control PEG-polyAlb groups at doses of 20 and 40 mg per kg were 766 ± 161 and 623 ± 99 seconds, respectively. At the dose of 40 mg per kg, the H12-PEG-polyAlb significantly reduced the bleeding time in comparison with controls.

Prolongation of hemostatic ability

The tail bleeding time of the thrombocytopenic rats before administration of H12-PEG-polyAlb or saline was 624 ± 175 seconds. The bleeding times at 5, 60, 180, and 360 minutes after administration of H12-PEG-polyAlb at a dose of 40 mg per kg were significantly reduced to 354 ± 67, 395 ± 75, 330 ± 73, and 371 ± 47 seconds, respectively, compared with that of the saline group at the same timing intervals (687 ± 131, 671 ± 142, 712 ± 113, and 538 ± 115 sec, respectively) (Fig. 4). This effect lasted for at least 6 hours. At 12 hours after administration, the bleeding time was 683 ± 149 seconds and was not significantly different from that of the saline group (890 ± 384 sec).

DISCUSSION

We previously measured the tail bleeding time at 5 minutes after the injection of H12-polyAlb, and confirmed a dose-dependent reduction in the bleeding time.[31] We then also confirmed that the $t_{1/2}$ of the H12-polyAlb was estimated to be approximately 10 minutes. The data suggested that the H12-polyAlb was of limited use because the $t_{1/2}$ of the particles was extremely short.[31]

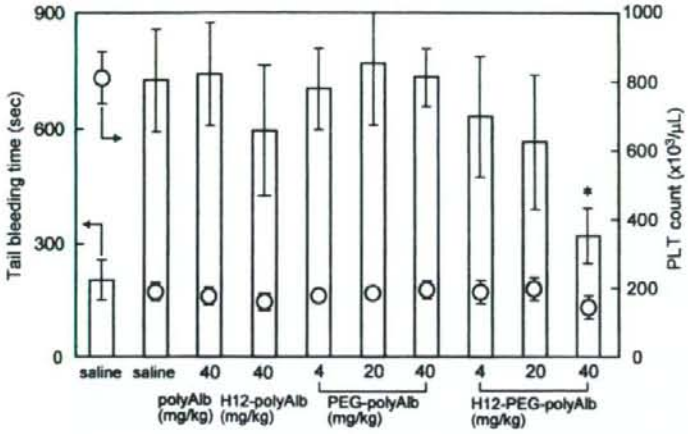

Fig. 3. Effects of the administration of H12-PEG-polyAlb on tail bleeding time at 180 minutes after injection (white bars). The administered amounts of H12-PEG-polyAlb was 4, 20, and 40 mg per kg equivalent of rHSA. (○) PLT concentration in the rats (n = 6-10). *p < 0.05 for H12-PEG-polyAlb versus PEG-polyAlb group at the same dose.

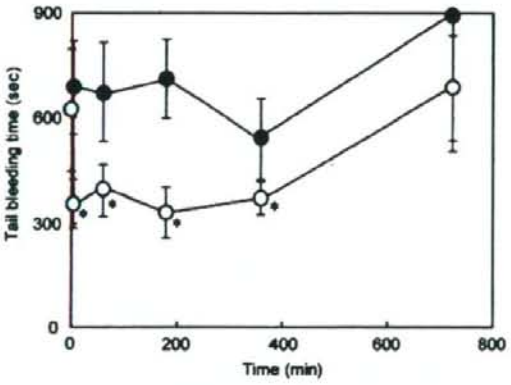

Fig. 4. Prolongation effect of hemostatic ability of H12-PEG-polyAlb on tail bleeding time (n = 5-8). H12-PEG-polyAlb (○) at 40 mg per kg equivalent of rHSA and saline (●) were administered, and tail bleeding time was measured at various time intervals after injection. *p < 0.05 for H12-PEG-polyAlb versus saline group at the same time intervals.

As noted in the introduction, PEG modification of intravenously injectable carriers has been widely used to prolong the $t_{1/2}$ or to stabilize their dispersion states.[32,33] We prepared polyAlb carrying both H12 and PEG chains to improve their stability for use in hemostasis as practical PLT substitutes.

The amount of the mPEG modifying the polyAlb increased with increasing addition of mPEG to the reaction mixture and reached saturation (Fig. 1), suggesting that PEG chains completely covered the surface of the polyAlb. The density of PEG on the particles, however, could be limited by the excluded volume effect of the neighboring PEG chains. For PEG of molecular weight 5.0 kDa, the excluded volume of the PEG chain can be estimated assuming a globular polymer chain to be of a diameter of 6.2 nm[37] If MALPEG and mPEG chains are considered to take a globular structure, which is a so-called mushroom structure, on the surface of polyAlb with a diameter of 200 ± 80 nm, the maximum number of PEG chains is estimated to 1.1×10^3. In the case of maximum PEG modification, however, the total number of PEG chains was estimated to 73×10^3, suggesting that MALPEG and mPEG chains likely take a so-called brush structure. This view was supported by results of other experiments which are briefly described below (data not shown). We used MALPEG with a molecular weight of 3.4 kDa instead of 5.0 kDa for modification of polyAlb, and modified mPEG (5.0 kDa), and then bound H12 to MALPEG modifying with the polyAlb to prepare H12-PEG-polyAlb. The modification number of mPEG increased with increasing addition of mPEG to the polyAlb, and for various preparations the number of the mPEG molecules per MALPEG-polyAlb particle was estimated to be approximately 13×10^3, 52×10^3, 78×10^3, and 112×10^3 molecules. The H12-PEG-polyAlb enhanced the ADP-induced PLT aggregation up to mPEG modification number of 52×10^3, indicating that the polyAlb cross-linked the activated PLTs to enhance the PLT aggregation. In the case of mPEG modification number of 78×10^3 or greater, however, the enhancement effect was significantly decreased, suggesting that MALPEG and mPEG chains were taking the so-called brush structure. In this structural arrangement, the functional interaction of H12 at the end of the MALPEG would be shielded because of the excluded volume effect of the neighboring mPEG chains, therefore contributing to the diminished effect of PLT aggregation with the highly modified particles noted above.

Furthermore, the conjugation number of H12 at the end of MALPEG was estimated to be approximately 10×10^3 at a yield of 52 percent, indicating that the maleimido groups of the MALPEG were exposed on the surface of the mPEG brush structures on the polyAlb. The conjugation density on the polyAlb surfaces was similar to that of H12-polyAlb which was shown to enhance PLT thrombus formation.[31] Also, the endotoxin concentration